Medical Physics
The International Journal of Medical Physics Research and Practice

High resolution gel-dosimetry by optical-CT and MR scanning

Mark Oldham, Jeffrey H. Siewerdsen, Anil Shetty, and David A. Jaffray

Citation: Medical Physics **28**, 1436 (2001); doi: 10.1118/1.1380430
View online: http://dx.doi.org/10.1118/1.1380430
View Table of Contents: http://scitation.aip.org/content/aapm/journal/medphys/28/7?ver=pdfcov
Published by the American Association of Physicists in Medicine

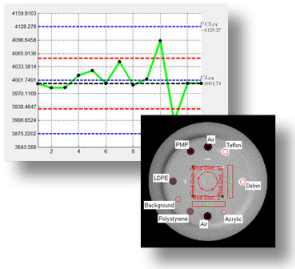

High resolution gel-dosimetry by optical-CT and MR scanning

Mark Oldham,[a] Jeffrey H. Siewerdsen, Anil Shetty, and David A. Jaffray
Department of Radiation Oncology, William Beaumont Hospital, 3601 W 13 Mile Rd, Royal Oak, Michigan 48073

(Received 27 October 2000; accepted for publication 19 April 2001)

The increased intricacy of Intensity-Modulated-Radiation-Therapy (IMRT) delivery has created the need for a high-resolution 3D-dosimetry (three-dimensional) system capable of measuring and verifying the complex delivery. Present clinical methods are inadequate being restricted to single points (e.g., ion-chambers) or to 2D planes (e.g., film), and are labor intensive. In this paper we show that gel-dosimetry in conjunction with optical-CT scanning can yield maps of dose that are of sufficient accuracy, resolution and precision to allow verification of complex radiosurgery deliveries, and by extension IMRT deliveries. The radiosurgery dose-distribution represents the most challenging case encountered in external beam therapy by virtue of the steep dose-gradients and high resolution of delivery. We characterize the stringent radiosurgery requirements by the RTAP (Resolution-Time-Accuracy-Precision) criteria defined as $\leqslant 1$ mm^3 spatial resolution, $\leqslant 1$ hour imaging time, accurate to within 3%, and within $\leqslant 1\%$ precision. The RTAP criteria is applied to an in-house laser-based optical-CT scanning system presented here, and evaluated using gel-flasks containing BANG3™ gel. The same gel flasks were subsequently imaged using the MR imaging protocol recommended by the gel manufacturer, but modified to match as closely as possible the RTAP. The resulting dose-maps demonstrate the high precision ($< 1.3\%$ noise at high dose) achievable with optical CT scanning while preserving high spatial resolution (<1 mm^3). Using the sequence above, the MR gel-dose maps were found to have poorer precision by a factor of 5, under the strict conditions of the RTAP. The optical CT gel-dosimetry system was further evaluated for the verification of a complex 3-isocenter radiosurgery delivery. In conclusion, this work demonstrates that gel-dosimetry and optical-CT scanning approach an important long-term goal of radiation dosimetry, as specified by the RTAP criteria, and have potential to impact the clinic by improving and facilitating clinical dose verification for the most complex external beam radiation treatments.
 [DOI: 10.1118/1.1380430]

Key words: Gel dosimetry, polymer gel, 3D dosimetry, optical CT scanning, radiosurgery

I. INTRODUCTION

A primary goal of radiation dosimetry has long been the development of an accurate, precise and efficient system that measures the dose in full three dimensions with high spatial resolution.[1] Such a system would have potential to impact radiation treatment verification as performed in the clinic. Two gel-dosimeters with the potential for full 3D dosimetry are in use and under development at the present time. The first is an extension of the well-established Fricke dosimeter, which was initially formulated as a solution to be examined by spectro-photometry.[2] Spatial information was obtained by Gore *et al.*[3] who proposed that the dose distribution could be probed by MR scanning rather than the conventional spectrophotometry. This breakthrough led researchers to ''fix'' the Fricke solution in a gelatinous matrix (the Fricke gel dosimeter) which then preserved the spatial distribution of the dose delivered to the gel. Subsequent scanning of the gel in an MR scanner yielded maps of the spatial distribution of T1 relaxation parameter which was observed to be proportional to the absorbed dose.[4,5]

Much research effort has gone into the development and utilization of the Fricke-gel dosimeter. The technique has not gained widespread acceptance into clinical practice however for two reasons. First the ferric ions (Fe3+) are small in dimension and were observed to diffuse through the gelatin matrix leading to degradation of the recorded dose distribution with time.[6] In practice the Fricke gel needs to be imaged within 1 h of irradiation which presents significant logistical problems to many clinics. Secondly the accessibility and cost of MR time required to image the Fricke gel often proves prohibitive. Despite these issues a thriving literature persists on the applications and research projects tackled with the Fricke gel dosimeter. These include investigations of single electron and photon beams (Back *et al.*[7]), bladder treatment (Johansson *et al.*[8]), abutting beams (Johansson *et al.*[8]), head-and-neck treatment (Scherer *et al.*[9]), dynamic wedge (Bengtsson *et al.*[10]), stereotactic and gamma knife treatment (Olsson *et al.*,[11] Chu *et al.*[12]) and brachytherapy treatments (Schreiner *et al.*,[13] Olsen *et al.*[14]).

A significant development occurred in 1993 (Maryanski *et al.*[15]) with the proposal of a polymer-gel dosimeter, which overcame the diffusion limitation associated with the Fricke gel.[16,17] We refer to polymer gels using the general term PAG (poly-acrylamide-gel) in the remainder of this paper. The basic mechanism of the PAG dosimeter is radiation-induced polymerization of bis and acrylamide. The resultant long chain-like molecules of bis-acrylamide were found to be too

large to diffuse through the gelatin matrix. Initial work on PAG dosimeters focussed on imaging the T2 relaxation rate distribution in the gel using an MR scanner. The R2 of the gel was found to be proportional to the amount of polymerization at that point in the gel, which was in turn proportional to the absorbed dose at that point.

The major advantage of the PAG is the lack of diffusion and, therefore, temporal stability of the dose-distribution recorded in the gel. Further advantages include tissue equivalence (Zeff=7.14), higher sensitivity, and energy and dose-rate independence within the clinical range.[17] These useful characteristics have led to the application the PAG dosimeter to numerous dosimetry issues in radiation therapy. Investigations have been summarized in a recent review article (McJury *et al.*[18]) and include simple geometry arrangements (Maryanski *et al.*[15,16]), characterization of brachytherapy sources (Ibbott *et al.*,[19] McJury *et al.*[20]), conformal therapy verification (De Deene *et al.*[21]), tomotherapy (Oldham *et al.*,[22] Low *et al.*[23]), radiosurgery (Meeks *et al.*[24]) and particle beam dosimetry (Ramm *et al.*,[25] Farajollahi *et al.*[26]). Baldock *et al.*,[27] reported a new approach to gel-dosimetry utilizing Raman spectroscopy to study changes in polymer cross-linking with dose. Improved techniques for gel-calibration were reported by Oldham *et al.*,[28] which yielded fourfold and tenfold lower uncertainties in the slope and intercept of the calibration curve.

At the present time much research effort is being directed to developing new methods of imaging the dose-distribution recorded in gel dosimeters.[29] The motivation is twofold. Firstly to find imaging techniques with less noise than is inherent in MR imaging. Secondly, to eliminate the reliance on MR technology with associated issues of limited access, and high scanning cost. Gore *et al.*[30] proposed a novel method to image PAG dosimeters by the technique of laser based optical-CT scanning. The optical-CT scanning approach was then applied by Kelly and Jordan *et al.*[31] to imaging a Fricke-benzoic-xylenol gel. This clever approach involved doping the Fricke gel with a radiochromic dye, and using the optical-CT scanning technique to map radiation-induced changes in local optical absorption coefficient.

Research into optical-CT imaging of gel dosimetry is thriving at the present time, and many aspects are in the early phases of development. Current publications in the literature are few and have been limited to demonstrations of optical-CT scanning in two dimensions.[30,31] Preliminary work by Oldham *et al.*[32,33] evaluated MR scanning with an in-house optical-CT scanning system for commercially available BANG3™ gel[1]. The BANG3™ gel has both a strong optical and MR response and was, therefore, well suited for this evaluation study. The results demonstrated a significant improvement in signal-to-noise ratio for the optical-CT technique when compared with a standard MR scanning approach [i.e., the MR scanning sequence recommended by the manufacturer of the gel-dosimeter, MGS Research (MGS Research, MGS Research Inc., P.O. Box 581, Guilford CT-06437 Tel: (203)245 32518)].

In this paper we report on a prototype optical-CT system designed and constructed at William Beaumont Hospital based on a first-generation model.[30,31] 2D images were obtained through selected planes of a gel-dosimeter, designed and constructed in collaboration with MGS Research, for use in a radiosurgery head-phantom verification system. The paper also describes a comparison of optical-CT scanning performance against a simple MR scanning method. The comparison focuses on sensitivity and accuracy of calibration, and imaging noise and resolution in dosimetric images. The important feature of the study is that each scanning method was applied to the same gel samples rendering direct comparison of the imaging modalities. The BANG3™ formulation was selected as the gel formulation of choice for this study as the nature of the radiation-induced polymerization causes a strong signal-change in both optical and MR modalities.[17,30]

A methodological difficulty arises when comparing two imaging modalities in that better results (i.e., higher signal-to-noise) can always be obtained by selecting longer imaging times and decreasing the spatial resolution of the images. Here we perform a meaningful comparison by setting limits on both spatial resolution and imaging-time. The key underlying concept for the comparison is that imaging parameters were selected to meet as closely as possible a Resolution-Time-Accuracy-Precision (RTAP) criteria. The RTAP criteria was defined with reference to the reasonable and ideal requirements for dosimetric verification of a radiosurgery delivery, namely spatial resolution <1 mm^3, imaging time <1 h, accurate to within 3%, and precision (noise) per pixel $<1\%$ (also see Schell *et al.*)[34] In practice, although the RTAP spatial resolution limit was achievable with the optical-CT scanner, only a $1\times1\times2$ mm^3 was achievable on the MR scanner due to sequence implementation limitations.

II. METHODS

Three identical near-cylindrical Barex flasks, designed and constructed in collaboration with MGS Research, were filled with BANG3™ gel also obtained from MGS Research Fig. 1(a). The flasks each held ~300cc of gel and were designed to be compatible with a radiosurgery head-phantom verification system [Figs. 1(b) and 1(c)], which allows reproducible positioning of the gel-flask within the water-filled head-phantom. Each flask was vacuum moulded (rather than conventionally blow-moulded) to preserve optical quality finish on the flask walls. The top of each flask was stopped with a delrin screw, into which a 1/4'' 20-pitch thread was tapped to allow mounting of the flask vertically in the optical scanner, and into the head-phantom [Fig. 1(c)]. The flat base of the flask was made from a 2 mm thick Barex sheet. Two of the flasks were used to investigate gel calibration issues, and the remaining flask was used as a dosimeter to study an intricate radiosurgical delivery.

A. Calibration irradiation

Each of the two calibration gel-flasks were placed upright in a water-bath and irradiated with three 6 MV radiosurgery beams shooting vertically upwards through the flat base. The beams were spatially offset to minimize contaminant cross-

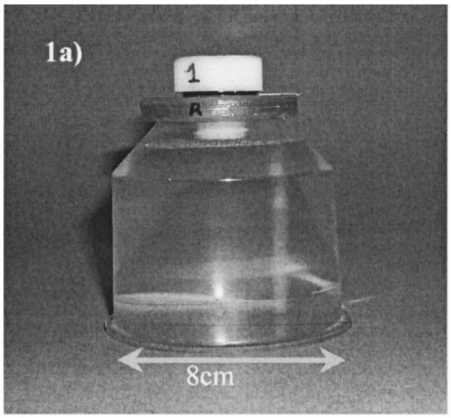

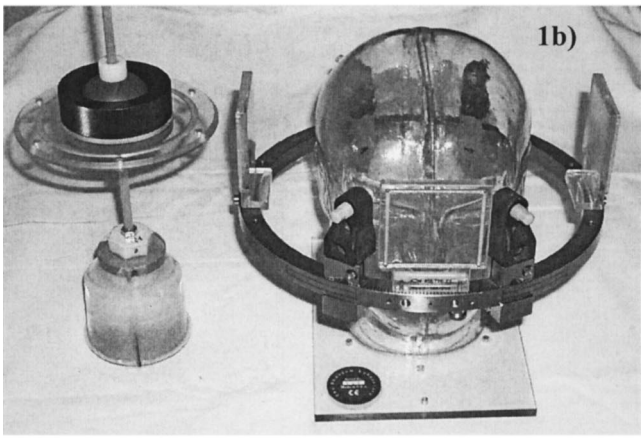

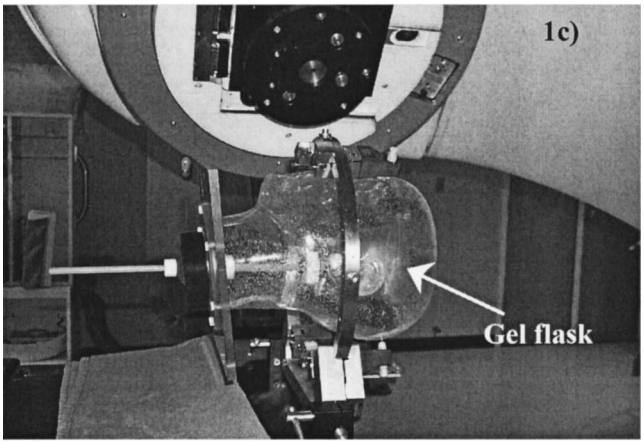

FIG. 1. (a) Barex gel-flask designed and constructed in collaboration with MGS Research, for use with the radiosurgery verification head phantom. (This flask was irradiated with a 2 mm diameter radiosurgery pencil beam, visible on the right side of the flask, to illustrate the optical contrast of the gel.) (b) Mechanism for mounting gel-flask inside the Beaumont radiosurgery verification head phantom. (c) Complete assembly mounted in treatment position.

scattered dose. The field size of the radiosurgery beam was 1.3 cm as defined by the 80% diameter at 5 cm depth. In the plane of maximum dose, the three beams delivered doses of 0.25, 0.75, and 1.5 Gy in the first flask and 0.5, 1.0, and 1.25 Gy in the second flask. The flasks were then scanned by both imaging modalities within 48 hours of irradiation (details in Sec. II C). Calibration data were obtained by noting the delivered dose at the maximum depth of each beam and the average pixel reading over a small region (5×5 mm^2) in the center of each beam. Pixel values were of R2(s^{-1})(=1/T2) in the MR image, and optical-attenuation μ (mm^{-1}) in the OCT image. The standard deviation on the average pixel value was taken to indicate the precision of the dosimeter imaging modality. Pixel values for unirradiated gel were determined from a separate unirradiated gel-flask.

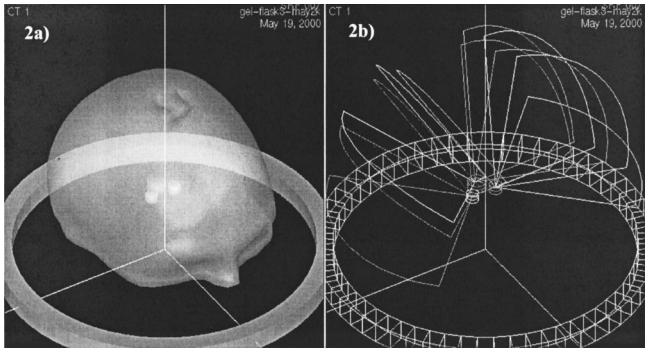

FIG. 2. 3D rendered surface of the radiosurgery head-phantom of Fig. 1, illustrating the three isocentre delivery (a) and the radiosurgery treatment arcs (b).

The calibration method outlined above is robust and insensitive to sources of error in the dose calculation (i.e., the dose from a single radiosurgery beam can be accurately calculated in this simple geometry) and in imaging of the gel-response. The maximal spacing and very steep penumbra of the radiosurgery beams minimizes cross-contamination. The depth-dose and x plane profiles of the radiosurgery beams were well known from beam commissioning data taken with a radiosurgery diode, pinpoint ion chamber, and radiographic film. The cylindrical geometry of the gel-dosimeter minimizes edge effects in both optical-CT and MR imaging (discussed further in Sec. II C).

B. Experimental irradiation

The remaining gel-flask was irradiated within a water-filled head-phantom (The Phantom laboratory, Salem, New York, USA.) specifically designed for verification of the radiosurgery technique. The flask is shown mounted inside the radiosurgery head-ring fixation system in Fig. 1(c). The combined head-phantom and interior gel-flask assembly was taken through the entire radiosurgery procedure mimicking the treatment of a patient. CT scan verifications of the phantom assembly when mounted both upright and up-side down, demonstrated negligible movement of the position of the flask inside the head-phantom within the limits of detection ($\sim$0.2 mm). A treatment plan was designed using the STP planning system (Stryker-Leibinger, 4100 East Milham Avenue, Kalamazoo, MI 49001-6197 USA) consisting of 3 isocentres to simulate a complex radiosurgery treatment. A 3D view of the isocentres and radiosurgery arc orientations is

shown in Fig. 2. The three isocenter treatment was then delivered to the phantom-flask assembly, using 6 MV radiation from a Varian Clinac 2100c.

C. Gel scanning by optical-CT and MR modalities

An important consideration is the stability of the irradiated gel and the time delay between gel-irradiation and gel scanning. A recent report on an in-house PAG dosimeter indicated that gel characteristics can vary significantly with time,[35] however a more stable behavior was observed in another in-house PAG dosimeter.[36] (Note: These in-house gels respond to radiation via the same mechanisms as the commercial. Slight differences in manufacturing technique can lead to differences in sensitivity but the physical mechanisms and limitations (e.g., sensitivity to oxygen contamination) are the same.) In the present work stability was not a significant concern as the main polymerization reactions for BANG3™ are completed within 15 min. After this time a slow and continuous ''creep'' may be observed for all R2 values in gel. The creep manifests as a gradual increase in R2 with time at all dose levels and has been attributed to the creation of radiation induced long-lived free radicals on the gelatin molecules.[37] The magnitude of the creep in the optical CT dose response is a 0.02% day change in slope, and an optical density change of 0.002/day in the intercept baseline.[38] To avoid minor complications associated to creep, both the optical and MR scanning measurements were made within 48 hours of irradiation.

1. MR scanning

All three flasks were imaged simultaneously in a 1.5 T Siemens Vision scanner. Initial imaging attempts were made with the flasks immersed in a water bath, but significant T2 artefacts in the free water rendered the images useless. These artefacts are attributed to macroscopic flow in free water associated to vibrations and were not related to the choice of scanning sequence. The flasks were thus imaged upright on a flat lucite sheet positioned horizontally in the head-coil so that the flasks were centerd in the magnetic field. Three coronal image planes were then scanned at selected depths in the flasks. The MR scanning sequence used was that recommended by MGS Research (the manufacturer of the BANG3™ gels) adjusted to meet as closely as possible the RTAP criteria. In practice the smallest slice-thickness implemented on the scanner was 2 mm for this sequence which violated the RTAP spatial criteria of 1 mm.

The in-plane spatial resolution was set at 0.98×0.98 mm. Details of the MR scanning procedure are as follows. Two Hahn spin echo (single echo) images were taken with TR of 1000 ms, and two different TE echo times. The first acquisition used TE=20 ms (a proton density image, which also carries information on spatial nonuniformities of the flip angle and of the coil sensitivity). The second acquisition used TE=100 ms (a heavily T2-weighted image, carrying information on dose distribution). The transmit and receive gains were kept constant for both acquisitions. Magnetization cross talk between neighboring slices was not a concern as the three coronal slices were separated by ~2 cm. High signal to noise was attempted by (i) using the high-sensitivity head-coil, (ii) positioning the gel centrally in the coil, in the region of maximum field homogeneity, and (iii) using as much signal averaging as possible in the time available. 3 NEX (a single acquisition=1 NEX) were used for the TE=20 ms echo and 5 NEX were used for the weaker TE=100 ms echo.

Transverse nuclear magnetic resonance (NMR) relaxation rates (R2=1/T2) of the water protons in the BANG gels are proportional to dose (R2=R0+kD) in the working range of the gel between 0 and 1.5 Gy. R2 maps were created from the two Hahn-spin-echo images acquired above by applying the following equation:

$$R2=[1/(TE2-TE1)]^{*}\log[S(TE1)/S(TE2)].$$

Where TE2=100 ms, S(TE2)=signal strength for TE2 image, TE1=100 ms, and S(TE1)=signal strength for TE=100 ms.

Although the MR imaging sequence outlined above has found widespread use in the literature,[23,24,39] several authors have reported improved MR scanning sequences, e.g., the CPMG.[40] The CPMG sequence was not available at the time of publication on our Siemens 1.5T Vision. As many centres, like us, do not have access to these advanced sequences the MR data presented here pertains to that obtainable by this basic imaging sequence. It is likely that more advanced sequences will produce superior images to those illustrated here.

2. Optical-CT scanning

The prototype optical-CT scanning system built for this work is illustrated in Figs. 3(a)–3(c). The system consists of a base-plate on which was mounted a uniphase 532 nm green HeNe 1.5 mW laser (Anderson Lasers Inc, 2882 W Royalton Rd, Broadview Hts, OH 44147) and a standard photodiode-lab-sphere assembly [PIN-10DP photodiodes obtained from (UDT Sensors Inc, 12525 Chadron Av., Hawthorne CA 90250.)] on opposite sides of a stationary water–bath of dimension $12 \times 12 \times 25$ cm. The diameter of the laser beam was reduced to 0.75 mm by means of a circular collimating aperture placed upstream of the water–bath. Collimating the width of the laser beam increases spatial resolution and reduces scattering in the water–bath. The base plate was mounted on a linear translation stage and translates as indicated in Fig. 3(a). Laser light is attenuated by the water–bath and gel-flask in the beam, and the amount of attenuation is measured by the photodiode.

Optical-CT scanning was performed as follows. First optical matching between the anti-freeze in the water-bath and the un-irradiated gel was achieved by diluting the antifreeze with distilled water until the deflection of the laser-beam under translation across the flask was minimized. Green antifreeze was chosen because it has a relatively high refractive index but allows passage of green light. Negligible deflection can be achieved except at the edges of the flask where strong refraction occurs. This ''edge effect'' manifests as a high

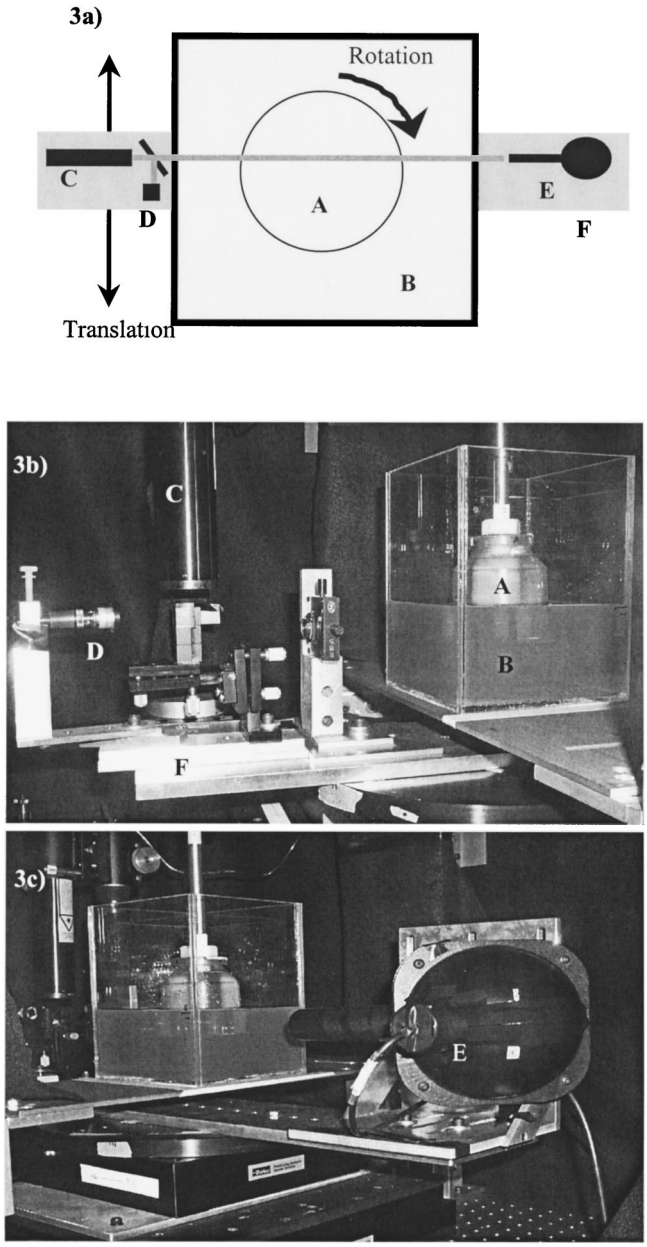

FIG. 3. Optical CT scanning apparatus: (a) schematic view from top, (b) left side of scanner, (c) right side of scanner. Labels are A=gel-flask, B=optically matched water–bath, C=laser, D=reference photo-diode, E=lab-sphere-field photo-diode assembly, F=base plate.

attenuation ring-artifact in the reconstructed image corresponding to the position of the walls of the flask. However as the edge effect is present in the reconstructed image of a gel-flask both before and after irradiation, the effect can be eliminated by a simple subtraction of the pre-irradiation image from the post irradiation image (see below). Horizontal line scans were taken where the laser was stepped in 1 mm increments across the flask with an additional 1.5 cm either side, allowing padding for the reconstruction. The flask was rotated by 1.8 degrees between each line-scan. Each completed line-scan constitutes a single projection through the gel. 100 such projections were acquired corresponding to 180 degrees of projection data. The total scanning time was about 20 minutes. The scanning parameters presented here represent a combination of hardware limitations and empirical experience to approach the RTAP criteria. The smallest angular increment of the rotational motor was 0.9 degrees, but the 1.8 degree interval was found to yield acceptable reconstructed images with respect to the RTAP criteria. The 1.8 degree interval was also preferred because scanning time is proportional to the number of projections. Great care was taken to align and ensure reproducible positioning of the gel-flask in the optical-CT scanning system. Reproducibility of <1 degree was achieved by aligning marks on the phantoms to positioning lasers rigidly incorporated into the structure of the optical-CT system. Reproducibility of $<1/2$ mm was achieved in the vertical dimension by the use of stopper rings on the shaft mounting the flask into the rotational motor.

The optical CT acquisition scanning software (in-house C++ code) was configured to return the ratio $R=I_{\mathrm{Ref}}/I_t$, i.e., the ratio of the laser intensity measured by the reference diode to the attenuated laser intensity measured by the field diode (Fig. 3). Optical-CT projection data was taken for the same slices in the phantom both pre and post irradiation of the gel-flask. A MATLAB script was written to reconstruct 2D images of the optical attenuation within the gel using the MATLAB implementation of the inverse-radon transform on the natural logarithm of the ratio R. Differential images (post-irradiation—pre-irradiation) were then obtained to yield a map of the changes in optical attenuation within the gel. Forming the subtraction image conveniently negates artefacts that are present in both original images (e.g., flask wall and reflection artefacts).

III. RESULTS AND DISCUSSION

Comparative transaxial images through a calibration flask illustrating three radiosurgery calibration beams are shown in Fig. 4. (All images presented here are un-processed with no smoothing or interpolation, in order to meet the spatial aspects of the RTAP criteria). The reduction in noise in the optical-CT image is dramatic when compared with the corresponding image from the MR scanner. The noise reduction is illustrated further in Fig. 5, where line profiles (orientation illustrated in Fig. 4) are compared for the optical-CT and MR modalities. In the higher dose peak, the signal to noise is estimated at 6.6% for MR (taking into account the baseline signal in the MR image) and 1.3% for optical CT. These values were obtained from average values over the central region in the peak. The high-noise exhibited in the MR image is significantly worse than that observed in a recent publication (Meeks *et al.*[24]) which uses the same MR imaging technique. The apparent discrepancy is resolved by noting two points. Firstly the signal-to-noise ratio in MR is to good approximation proportional to voxel size. In the present work the voxel size was set at 2 mm^3 ($1\times1\times2$ mm), as close as possible to the RTAP criteria. This is nearly a factor of 4 smaller than the $1.56\times1.56\times3$ mm used in Ref. 24. Secondly, no smoothing algorithms have been applied to the present images, whereas a Gaussian smoothing filter (3 pixel

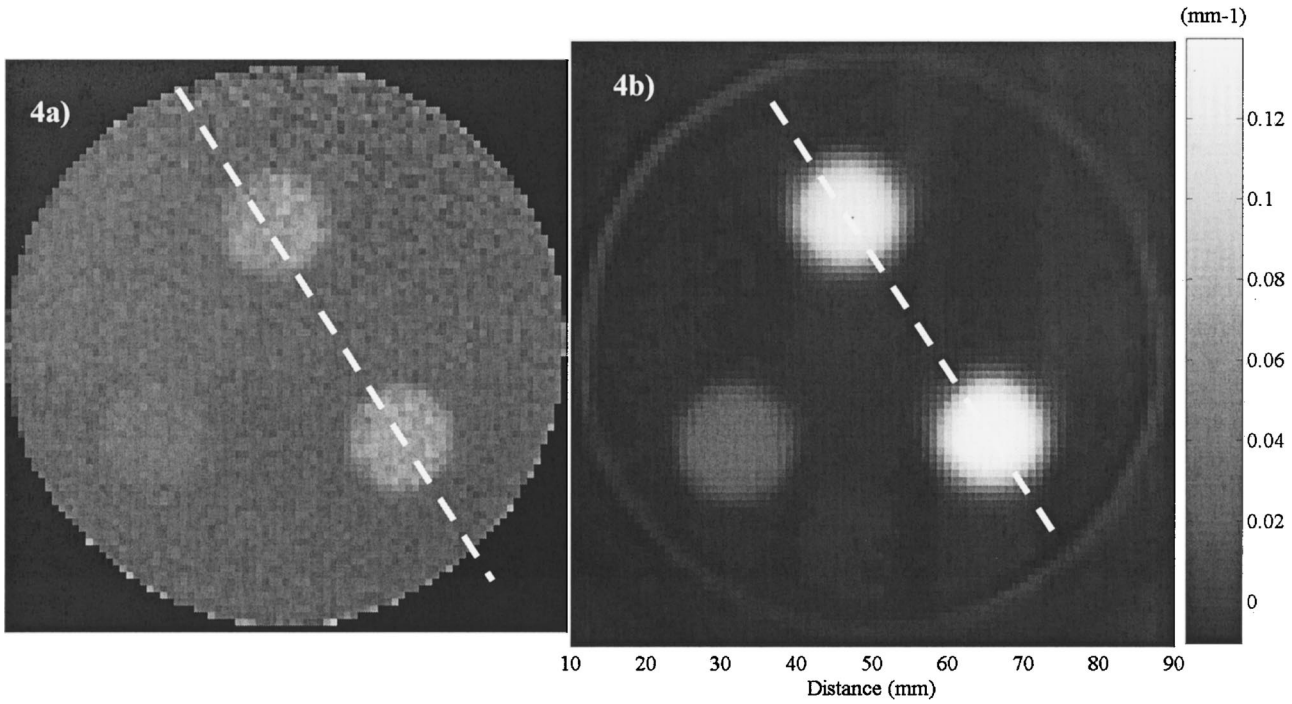

FIG. 4. Unprocessed transaxial images through the same plane of *the same* calibration gel-flask (a) MR image of the R2 distribution, (b) optical-CT image of the change-in-optical-attenuation. The dotted line indicates the line profile of Fig. 5.

width, 1 pixel sigma) was applied in Ref. 24. Together the factor of four larger sampling volume and the application of the Gaussian filter explain the improved image quality and lower noise reported in the latter. Although smoother images are obtainable with a variety of smoothing algorithms the use of such numerical filtering is restricted if the strict RTAP criteria are to be met. Whilst they reduce the noise in the image, smoothing algorithms also reduce the spatial accuracy and resolution in the regions of particular interest (i.e., regions of steep gradient).

The calibration plots for MR and optical scanning are shown in Figs. 6(a) and 6(b). The figures show the measurement of the active parameter ($\Delta\mu$ the change in optical attenuation for optical-CT, and R2 for MR) versus dose for the

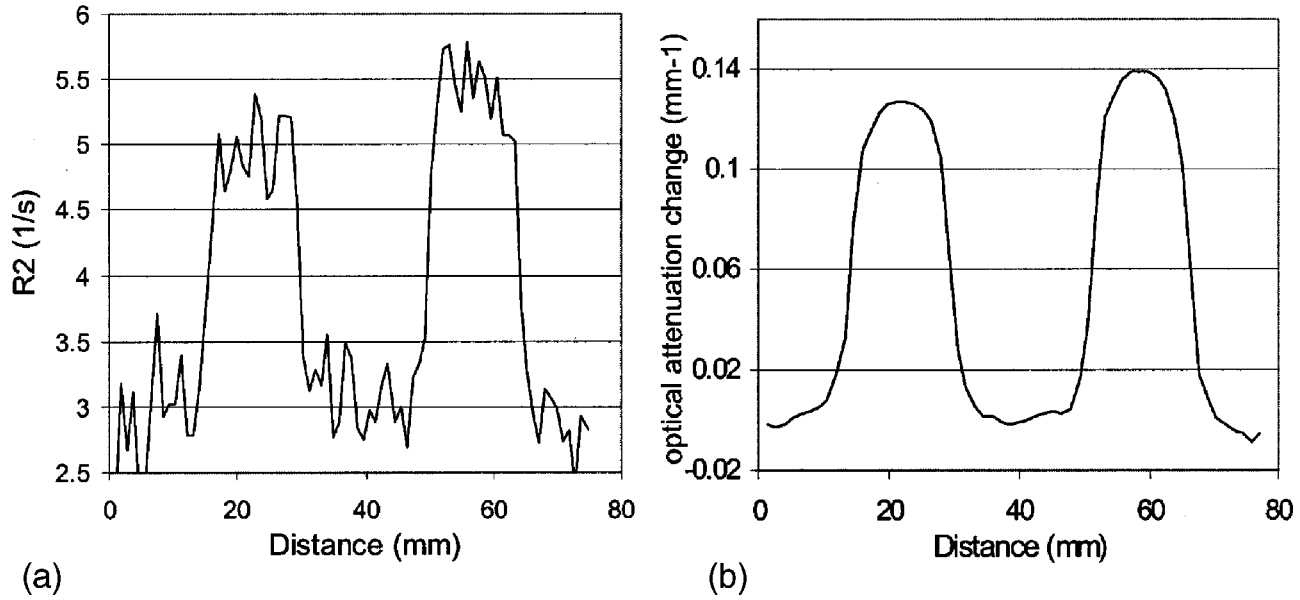

FIG. 5. Line profile along the trajectory illustrated in Fig. 4, for the same gel-flask, imaged by MR scanning (left image) and optical-CT (right image). The profiles illustrate the high precision obtained with the optical CT scanner.

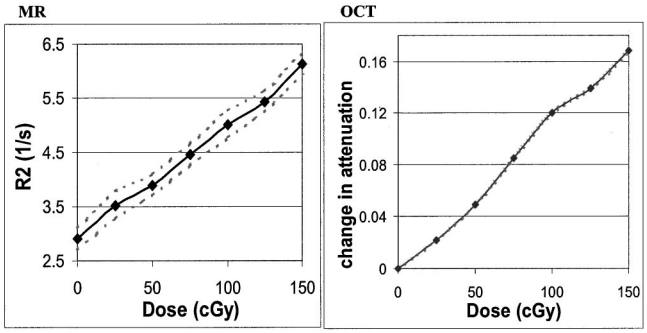

FIG. 6. Calibration data for the same gel flasks. The MR calibration response is the left hand image and the optical response is on the right. The dotted lines indicate 1 SD bounds on individual points.

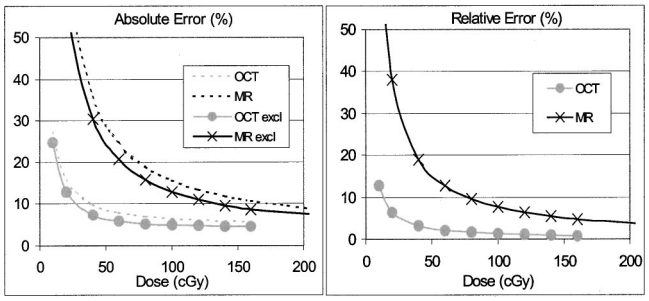

FIG. 7. Comparison of absolute and relative uncertainties on dose measurement. The ordinate is the percentage uncertainty on the dose measured with the gel dosimeter. The dashed curves correspond to the upper bound by inclusion of the cross-correlation term in Eq. (2). The solid curves exclude this term.

6-radiosurgery calibration beam deliveries. The measured values and standard deviation of measurement

$$Dose = \alpha x_i + \beta,$$
$$x = R2, \quad MR, \tag{1}$$
$$x = \mu, \quad OCT,$$

were obtained from a sample area of ~25 pixels in the center of the beam (i.e., 5×5 mm). The reduction in 1 SD bounds illustrated in Fig. 6 is a consequence of the higher signal to noise observed in the optical-CT images.

A measure of the accuracy of calibration for both the MR and optical-CT modalities is determined from the uncertainty on the linear calibration fit [Eq. (1)]. These uncertainties are given in Table I. Dividing the uncertainty on any single value (σ_i in Table I) by the maximum signal confirms the percentage uncertainty at peak signal of ~1.2% and ~6.0% for optical-CT and MR, respectively. Interestingly, the factor of nearly six lower noise in the optical-CT data does not translate into less uncertainty on the slope of the fit (σ_α). This is evidence for a small systematic effect in the optical-CT dose-calibration data visible as the slight deviations from linearity in the optical-CT calibration data in Fig. 6. The effect warrants further study but a possible explanation is an imperfect alignment of the mounting thread in the delrin screw-top with the axis of the gel-flask, causing the scanning laser to move out of plane with rotation of the gel flask.

The calibration uncertainties in Table I transmit through to uncertainties on dosimetric measurements made with the gel dosimeter. Quantification of the error is found by evaluating the error propagation expression for the percentage error on dose [Eq. (2)].[39] Inserting the measured uncertainties (Table I) into Eq. (2) yield the relative and absolute uncertainty plots for dose measurements made with the gel dosimeter Fig. 7. It is noted that for relative dosimetry $\sigma_\alpha = \sigma_\beta = 0$.

$$\frac{\sigma_D}{D} \leqslant \sqrt{\left(\frac{x\sigma_\alpha}{D}\right)^2 + \left(\frac{\alpha\sigma_x}{D}\right)^2 + \left(\frac{\sigma_\beta}{D}\right)^2 + \frac{2x\sigma_\alpha\sigma_\beta}{D^2}}. \tag{2}$$

Figure 7 illustrates the superior accuracy achievable with the optical-CT scanning approach, when constricted by the RTAP criteria. Two absolute error curves are shown for each imaging modality, corresponding to the inclusion or not of the cross-correlation term in Eq. (2). The cross-correlation term quoted in Eq. (2) is an upper estimate[39] and the dashed lines in Fig. 7, therefore, represent an upper bound of the error. The effect of this term has been ignored in previous articles.[28,41] The error curves for the MR data are shown extrapolated to higher doses. This is in recognition that the MR signal of the gel saturates at higher doses than the optical signal. The gel becomes sufficiently opaque at doses above 1.5 Gy to render the gel unsuitable for optical scanning. However, the MR response continues linearly above this threshold to above 2 Gy, and saturation does not occur until about 3 Gy. The extrapolated curves in Fig. 7 are valid because the linear fit extends to these doses and because the uncertainty on individual measurements is independent of the dose. A limitation of this study is the restriction of the doses to the useable optical range of the gel. However, it is important to note that the R2 range covered by the data in this work is still particularly high, and is significantly greater than the full-range reported by several in-house PAG dosimeters.[22,42,43]

From Fig. 7, the gel dosimeter, when scanned optically, is capable of dose measurement with uncertainty of ~1.1% when used to measure the relative dose-distribution. This figure increases to about 4% for absolute dose measurement. In the MR scanning approach, an uncertainty of about 4.5% is incurred in the relative distribution, which increases to about 10% for absolute dosimetric measurement. These uncertainties are higher than have been quoted in other reports[18] but the apparent discrepancies are explained, as outlined earlier with reference to Ref. 24, by the fact that in the present work the MR technique was pushed to meet the

TABLE I. uncertainties on the calibration regression fit of Eq. (1). σ_i, the uncertainty on an individual measurement, was found to be independent of dose in the MR data, and to gradually increase with dose over the range shown in the OCT data.

	OCT	MR
σ_α	4.4%	2.7%
σ_β	±4 cGy	±6 cGy
σ_i	0.0005–0.0015 (mm^{-1})	0.2 (s^{-1})

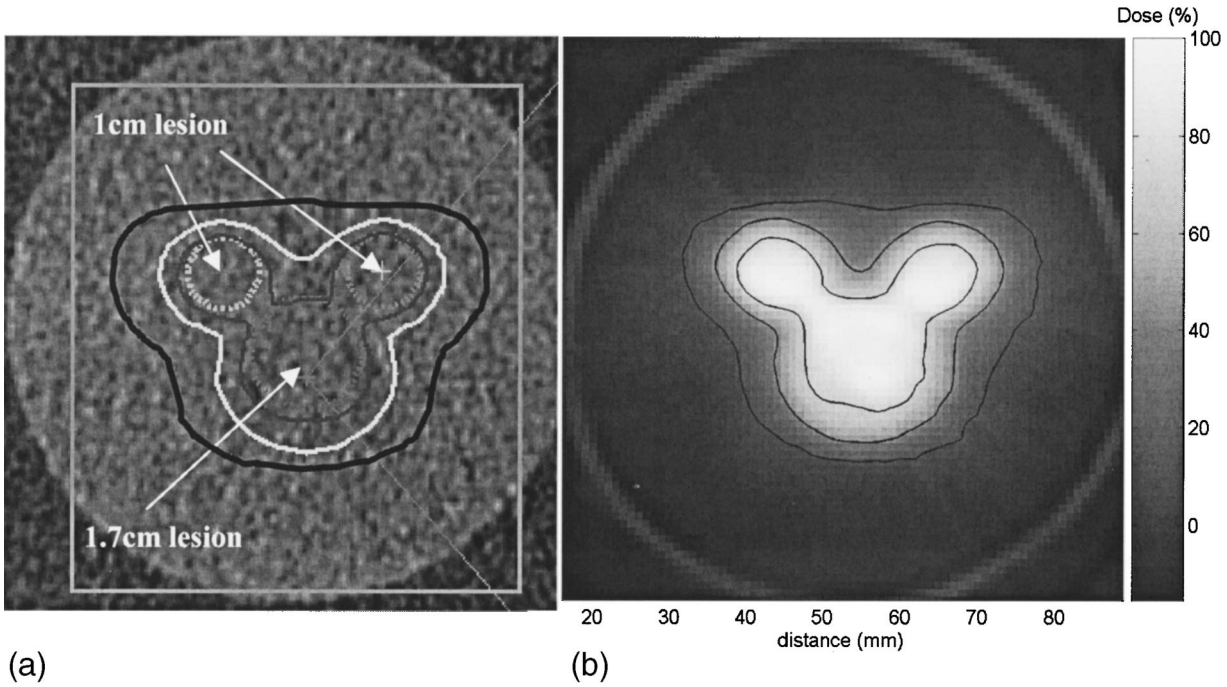

FIG. 8. Figure illustrates the use of the gel-dosimeter in conjunction with optical-CT scanning to verify a three isocenter radiosurgery treatment. The left hand image is the computer modeled distribution (isodoses 80%, 50%, and 20%) superimposed onto the CT scan of the head-phantom. The right hand image is a dose map obtained from optical CT scanning through the central plane of the distribution (lines are also 80%, 50%, and 20%).

RTAP criteria. Noise exhibited in the MR dose map increases when the spatial resolution is reduced to 1 mm^3, when no smoothing algorithms are applied, and when a one hour imaging time limit is set. In regions of lower dose the percentage uncertainty increases for both modalities as indicated in Fig. 7.

The dosimetric use of the gel-dosimeter is illustrated for the verification of a three isocenter radiosurgery delivery in Fig. 8. The left hand image is the predicted distribution from the STP planning system (isodoses 80%, 50%, and 20%) superimposed onto the CT scan of the head-phantom. The STP dose-algorithm is known to model the radiosurgery dose delivery with high accuracy (i.e., to the accuracy of the original commissioning measurements), in the absence of significant inhomogeneities and obliquity, because it reproduces the commissioned beam data for the appropriate radiosurgery collimator. The left image in Fig. 8 is therefore taken as the gold-standard against which the gel-dosimeter can be compared. The right hand image is a dose map obtained from optical CT scanning through the central plane of the distribution (lines are also 80%, 50%, and 20%). The unsmoothed gel dose-map image is of high quality. The smooth and unbroken isodose lines allow detailed comparison with the planned distribution, and are a significant improvement on other high-resolution gel dose-map images obtained with MR.

The scanner design presented here is restricted to a single narrow laser beam that is scanned across the gel. A substantial decrease in scanning time could be achieved by moving to a broad-beam geometry. However, the scattering nature of the BANG3™ gel prevents this approach due to the difficulty in resolving the trajectory of scattered light. Progress in this area requires the development of absorbing rather than scattering gel-dosimeters, of which several are in development at the present time.[29,44]

IV. CONCLUSIONS

The data shown here support the conclusion that gel dosimetry in conjunction with optical-CT scanning can produce 3D dose-maps of sufficient quality (resolution, accuracy and precision) for the verification of even the most stringent dosimetric challenges posed by radiosurgery and new IMRT techniques. The signal-to-noise ratio in the optical CT image was $<1.3\%$ in high dose regions, which compares favorably with 5% to 6% observed in the MR data obtained using a simple MR imaging sequence (Sec. II C 1). The use of more advanced MR sequences may be able to improve on the latter figure. The low noise achieved in the optical-CT scanning technique is a consequence of the sensitivity and precision of the photodiode technology used to measure transmitted laser light. The noise in the MR scanning technique presented here is higher than reported in other work[24] using the same MR imaging sequence but different parameter settings. The apparent discrepancy is resolved by noting that the higher noise observed in the present work is a consequence of selecting higher spatial resolution and avoiding the use of image-smoothing filters. Both of these are requirements if the RTAP criteria is to be met. In conclusion, we believe the optical-CT gel-dosimetry system approaches a major goal of dosimetry: A 3D dose mapping system that meets the RTAP criteria (<1 mm resolution, <1 hour imaging time, 3% accuracy, and

<1% precision). As such the system has potential to impact dosimetric verification as presently performed in the clinic. The potential clinical benefits are significant, and include facilitating clinical implementation of complex radiosurgery and new IMRT stereotactic techniques.

[a]Electronic mail: moldham@beaumont.edu

[1] S. Webb, *Intensity Modulated Radiation Therapy: Verification of 3D Dose Distributions*, Inst. of Physics Publishing, 2001.

[2] H. Fricke and E. J. Hart, ''Chemical dosimetry,'' *Radiation Dosimetry Vol. 2*, edited by F. H. Attix and W. C. Roesch (Academic, New York, 1966).

[3] J. C. Gore, Y. S. Kang, and R. J. Schultz, ''Measurement of radiation dose distribution by nuclear magnetic resonance imaging,'' Phys. Med. Biol. **29**, 1189–1197 (1984).

[4] L. E. Olsson, A. Fransson, A. Ericsson, and S. Mattsson, ''MR imaging of absorbed dose distributions for radiotherapy using ferrous sulphate gels,'' Phys. Med. Biol. **35**(12), 1623–1631 (1990).

[5] P. V. Prasad, O. Nalcioglu, and B. Rabbani, ''Measurement of three-dimensional radiation dose distributions using MRI,'' Radiat. Res. **128**(1), 1–13 (1991).

[6] B. J. Balcom, T. J. Lees, A. R. Sharp, N. S. Kulkarni, and G. S. Wagner, ''Diffusion in Fe(II/III) radiation dosimetry gels measured by MRI,'' Phys. Med. Biol. **40**, 1665–1676 (1995).

[7] S. A. Back, P. Magnusson, L. E. Olsson, A. Montelius, A. Fransson, and S. Mattsson, ''Verification of single beam treatment planning using a ferrous dosimeter gel and MRI (FeMRI),'' Acta Oncol. **37**(6), P561–P566 (1998).

[8] S. A. Johansson, P. Magnusson, A. Fransson, L. E. Olsson, J. O. Christoffersson, A. Montelius, and S. Mattsson, ''Dosimeter gel and MR imaging for verification of calculated dose distributions in clinical radiation therapy,'' Acta Oncol. **36**, 283–290 (1997).

[9] J. Scherer, L. Bogner, M. Herbst, and A. Muller-Broich, ''Verifikation optimierter 3D-dosisverteilungen mittels mr-fricke-gel,'' Strahlenther Onkol **173**, 36–42 (1997).

[10] M. Bengtsson, T. Furre, J. Rodal, A. Skretting, and D. R. Olsen, ''Measurement of dynamic wedge angles and beam profiles by means MRI ferrous-sulphate gel dosimetry,'' Phys. Med. Biol. **41**(2), 269–277 (1996).

[11] L. E. Olsson, J. Arndt, A. Fransson, and B. Nordell, ''Three-dimensional dose mapping from gamma knife treatment using a dosimeter gel and MR-imaging,'' Radiol. Oncol. **24**, 82–86 (1992).

[12] W. C. Chu, W. Y. Guo, M. C. Wu, W. Y. Chung, and D. H. Pan, ''The radiation induced magnetic resonance image intensity change provides a more efficient three-dimensional dose measurement in mri-fricke-agarose gel dosimetry,'' Med. Phys. **25**, 2326–2332 (1998).

[13] L. J. Schreiner, I. Crooks, M. D. Evans, B. M. Keller, and W. A. Parker, ''Imaging of HDR brachytherapy dose distributions using NMR Fricke-gelatin dosimetry,'' Magn. Reson. Imaging **12**, 901–907 (1994).

[14] D. R. Olsen and J. Hellesnes, ''Absorbed dose distribution measurements in brachytherapy using ferrous sulphate gel and magnetic resonance imaging,'' Br. J. Radiol. **67**, 1121–1126 (1994).

[15] M. J. Maryanski, J. C. Gore, R. P. Kennan, and R. J. Schulz, ''NMR relaxation enhancement in gels polymerised and cross-linked by ionising radiation: a new approach to 3D dosimetry by MRI,'' Magn. Reson. Imaging **11**, 253–258 (1993).

[16] M. J. Maryanski, R. J. Schulz, G. S. Ibbott, J. C. Gatenby, J. Xie, D. Horton, and J. C. Gore, ''Magnetic resonance imaging of radiation dose distributions using a polymer-gel dosimeter,'' Phys. Med. Biol. **39**, 1437–1455 (1994).

[17] M. J. Maryanski, G. S. Ibbott, P. Eastman, R. J. Schulz, and J. C. Gore, ''Radiation-therapy dosimetry using magnetic-resonance imaging of polymer gels,'' Med. Phys. **23**, No. 5, 699–705 (1996).

[18] M. McJury, M. Oldham, V. P. Cosgrove, P. S. Murphy, S. Doran, M. O. Leach, and S. Webb, ''Radiation dosimetry using polymer gels: Methods and Applications,'' (Review Article), Br. J. Radiol. **73**, 919–929 (2000).

[19] G. S. Ibbott, M. J. Maryanski, P. Eastman, S. D. Holcomb, Y. S. Zhang, R. G. Avison, M. Sanders, and J. C. Gore, ''3D visualisation and measurement of conformal dose-distributions using MRI of BANG-gel dosimeters,'' Int. J. Radiat. Oncol., Biol., Phys. **38**, No. 5, 1097–1103 (1997).

[20] M. McJury, P. D. Tapper, V. P. Cosgrove, P. S. Murphy, S. Griffin, M. O. Leach, S. Webb, and M. Oldham, ''Experimental 3D dosimetry around a high-dose-rate clinical 192Ir source using a polyacrylamide gel (PAG) dosimeter,'' Phys. Med. Biol. **44**(10), 2431–2444 (1999).

[21] Y. De Deene, C. De Wagter, B. Van Duyse, S. Derycke, W. De Neve, and E. Achten, ''Three-dimensional dosimetry using polymer gel and magnetic resonance imaging applied to the verification of conformal radiation therapy in head-and-neck cancer,'' Radiol. Oncol. **48**(3), 283–291 (1998).

[22] M. Oldham, I. B. Baustert, C. Lord, T. A. R. Smith, M. McJury, M. O. Leach, A. P. Warrington, and S. Webb, ''An investigation into the dosimetry of a 9 field tomotherapy irradiation using BANG-gel dosimetry,'' Phys. Med. Biol. **43**(5), 1113–1132 (1998a).

[23] D. A. Low, J. F. Dempsey, R. Venkatesan, S. Mutic, J. Markman, E. Mark Haacke, and J. A. Purdy, ''Evaluation of polymer gels and MRI as a 3-D dosimeter for intensity-modulated radiation therapy,'' Med. Phys. **26**(8), 1542–1551 (1999).

[24] S. L. Meeks, F. J. Bova, M. J. Maryanski, L. A. Kendrick, M. K. Ranade, and J. M. Buatti, ''Friedman image registration of BANG gel dose maps for quantitative dosimetry,'' Int. J. Radiat. Oncol., Biol., Phys. **43**(5), 1135–1141 (1999).

[25] U. Ramm, M. Damrau, C. Thilmann, H. D. Bottcher, M. Kramer, O. Geiss, G. Kraft, J. Ahlswede, M. Bock, and L. Schad, ''3D heavy ion dosimetry using MRI of polymer gels, Proc. of the 1st Int. Workshop on Radiation therapy gel dosimetry,'' Lexington, July, USA, 1999.

[26] A. R. Farajollahi, D. E. Bonnett, D. Tattam, and S. Green, ''The potential use of polymer gel dosimetry in boron neutron capture therapy,'' Phys. Med. Biol. **45**(4), 9–14 (2000).

[27] C. Baldock, L. Rintoul, S. F. Keevil, J. M. Pope, and G. A. George, ''Fourier transform Raman spectroscopy of polyacrylamide gels (PAGs) for radiation dosimetry,'' Phys. Med. Biol. **43**(12), 3617–3627 (1998).

[28] M. Oldham, M. McJury, I. B. Baustert, S. Webb, and M. O. Leach, ''Improving calibration accuracy in gel dosimetry,'' Phys. Med. Biol. **43**(10), 2709–2720 (1998b).

[29] K. Jordan, ''Developmental issues for optical CT and gel dosimetry,'' Proc. of the 1st Int. Workshop on Radiation therapy gel dosimetry,'' Lexington, July, USA, 1999.

[30] J. C. Gore, M. Ranade, M. J. Maryanski, and R. J. Schulz, ''Radiation dose distributions in three dimensions from tomographic optical density scanning of polymer gels: I. Development of an optical scanner,'' Phys. Med. Biol. **41**(12), 2695–2704 (1996).

[31] R. G. Kelly, K. J. Jordan, and J. J. Batista, ''Optical CT reconstruction of 3D dose distributions using Ferrous benzoic-xylenol (FBX) gel dosimeter,'' Med. Phys. **25**, 1741–1750 (1998).

[32] M. Oldham, J. H. Siewerdsen, A. Shetty, and D. A. Jaffray, ''An investigation comparing optical-CT with MR scanning for polymer gel dosimeters,'' Proc. of the World Congress on Medical Physics, Chicago, USA, July 2000a.

[33] M. Oldham, J. H. Siewerdsen, and D. A. Jaffray, ''An initial investigation of optical-CT and MR scanning of gel dosimeters'' Proc. of the XIIIth Int. Conf. On the Use of Computers in Radiation Therapy, Heidelberg, Germany, May, 2000b.

[34] M. C. Schell *et al.*, Stereotactic Radiosurgery, Report of Task Group 42 Radiation Therapy Committee, American Association of Physicists in Medicine, June 1995.

[35] M. McJury, M. Oldham, M. O. Leach, and S. Webb, ''Dynamics of polymerization in polyacrylamide gel (PAG) dosimeters: (I)ageing and long-term stability,'' Phys. Med. Biol. **44**(8), 1863–1873 (1999).

[36] Y. De Deene, P. Hanselaer, C. De Wagter, E. Achten, and W. De Neve, ''An investigation of the chemical stability of a monomer/polymer gel dosimeter,'' Phys. Med. Biol. **45**(4), 859–878 (2000a).

[37] M. J. Maryanski, ''Radiation sensitive polymer gels: properties and manufacturing,'' Proc. of the 1st Int. Workshop on Radiation therapy gel dosimetry'' Lexington, July, USA, 1999.

[38] M. J. Maryanski, Private communication of unpublished data, 2000.

[39] D. A. Low, J. Markham, J. F. Dempsey, S. Mutic, M. Oldham, R. Venkatesan, E. M. Haacke, and J. A. Purdy, ''Noise in polymer gel measurements using MRI,'' Med. Phys. **27**(8), 1814–1817 (2000).

[40] I. C. Baustert, M. Oldham, T. A. Smith, C. Hayes, S. Webb, and M. O. Leach, ''Optimized MR imaging for polyacrylamide gel dosimetry,'' Phys. Med. Biol. **45**(4), 847–858 (2000).

[41] C. Baldock, P. Murry, and T. Kron, Uncertainty analysis in polymer gel dosimetry, Phys. Med. Biol. **44**(11), N243–N246 (1999).

[42] V. P. Cosgrove, P. S. Murphy, M. McJury, E. J. Adams, A. P. Warrington,

M. O. Leach, and S. Webb, ''The reproducibility of polyacrylamide gel dosimetry applied to stereotactic conformal radiotherapy,'' Phys. Med. Biol. **45**(5), 1195–1210 (2000).

[43] Y. De Deene, C. De Wagter, B. Van Duyse, S. Derycke, B. Mersseman, W. De Gersem, E. Voet, T. Achten, and W. De Neve, ''Validation of MR-based polymer gel dosimetry as a preclinical three-dimensional verification tool in conformal radiotherapy,'' Magn. Reson. Med. **43**(1), 116–125 (2000b).

[44] K. C. Chu, K. J. Jordan, J. J. Battista, J. Van Dyk, and B. K. Rutt, ''Polyvinyl alcohol-Fricke hydrogel and cryogel: two new gel dosimetry systems with low Fe3+ diffusion,'' Phys. Med. Biol. **45**(4), 955–969 (2000).